Modified Polyimide Side-Chain Polymers for Electrooptics

P. Prêtre, P. Kaatz, A. Bohren, and P. Günter*

Nonlinear Optics Laboratory, Institute of Quantum Electronics, Swiss Federal Institute of Technology, ETH Hönggerberg, CH-8093 Zürich, Switzerland

B. Zysset, M. Ahlheim, M. Stähelin, and F. Lehr

SANDOZ Optoelectronics Research, SANDOZ Huningue SA, F-68330 Huningue, France

Received April 28, 1994; Revised Manuscript Received June 22, 1994®

ABSTRACT: New modified polyimide polymers with pendent side group nonlinear optical (NLO) azo chromophores and moderate to high glass transition temperatures (140 °C < T_g < 190 °C) have been prepared. Corona poled films of these polymers possess large nonlinear optical susceptibilities of d_{31} = 23 pm/V and electrooptic (EO) coefficients of r_{13} = 6.5 pm/V at a wavelength of λ = 1.3 μm. The structural properties (glass transition, molecular weight, chromophore density) and optical properties (refractive index, optical nonlinearity) of these polyimides can easily be varied to fulfill the requirements of potential electrooptic devices. Due to the relatively high glass transition temperatures of these polymers, long-term stability of the optical nonlinearity of typically one to hundreds of years at operating temperatures of 80–100 °C is predicted from accelerated time–temperature measurements. Using a development of a phenomenological theory of the glass transition, a normalized relaxation law is proposed with $(T_g - T)/T$ as the relevant scaling parameter.

I. Introduction

In recent years a considerable amount of research has been directed toward the development of nonlinear optical (NLO) and electrooptic (EO) polymers. These polymers are thought to have considerable potential for efficient, ultrafast, and low voltage electrooptic modulators and related devices.[1] The frequently cited potential advantages of polymeric materials are high nonlinear optical coefficients, ease of processing, and device fabrication. Consequently, low production costs are envisioned for these materials. However, additional requirements must be satisfied before polymeric materials can demonstrate their potential as actual device materials. Some of these include good long-term stability of the NLO or EO effect, good structural and chemical stability, and low optical propagation losses. Recent reports in the literature have demonstrated that all of these properties can be achieved with polymeric materials, but presently no single polymer can satisfy all the requirements of current device specifications.[2]

Insufficient temporal stability of the induced polar ordering of NLO chromophores at elevated temperatures is a major hindrance to further progress in developing polymeric NLO devices.[3] Several different approaches have recently been proposed to solve this problem. Functionalized side-chain polymers where the NLO chromophore is covalently attached to the polymer backbone have been a typical approach, but others include thermal or photo-cross-linkable network polymers,[4-8] functionalized polymers where the NLO chromophore is incorporated into the polymer main-chain backbone,[9,10] and guest–host systems with polyimide polymers.[11-15] Generally, polymer systems with increased glass transition temperatures show improved temporal stability, although the efficacy varies depending on how the NLO chromophore is incorporated into the polymer matrix. Cross-linking the polymer matrix increases the glass transition temperature, but there are thermal degradation problems associated with the extended poling cycles required for thermal cross-linking and problems of photostability of typical NLO chromophores during photo-cross-linking processes. High temperature guest–host polyimide systems have demonstrated excellent thermal and temporal stability, but there are also undesirable effects associated with the limitations of low chromophore loading and the consequently smaller EO coefficients.

In this work we have prepared modified polyimide polymers with NLO side-chain azo chromophores with moderate to high glass transition temperatures (140 °C < T_g < 190 °C). These polymers offer the possibility of high chromophore densities and concomitant high SHG and EO coefficients. Extensive SHG time–temperature measurements have also been done to verify the degree of stability of the induced polar ordering in these polymer films. With the aid of a scaling relation, we find that the relaxation behavior of the NLO chromophores can be reasonably well modeled to a first approximation in terms of current phenomenological descriptions of the glass transition. A significant improvement of the long-term stability of the EO effect at device operating temperatures is found from these accelerated time–temperature measurements.

II. Side-Chain Polyimide NLO Polymers

The chemical structures of the polymers characterized in this work are shown in Figure 1. The amino–alkyl–amino functionalized NLO azo chromophores, with the various substitution patterns shown in Table 1, were attached via a two or three carbon spacer linkage to an alternating styrene–maleic anhydride copolymer. Three polymers denoted by A-095.11, A-097.07, and A-148.02 with the chromophores indicated in Table 1 were chosen for the detailed measurements described in this work. A discussion of the chemical synthesis is given elsewhere.[16]

Figure 2 shows the glass transition temperatures obtained by differential scanning calorimetry (DSC) measurements as a function of the molar chromophore concentration for the two or three carbon spacer linkage. These modified polyimide polymers have glass transitions that are about 20–60 deg higher than typical methacrylic NLO copolymers with, however, a pronounced plasticizing effect as a function of chromophore concentration. With nearly complete (90 mol % corresponding to 56 wt %)

® Abstract published in *Advance ACS Abstracts*, August 1, 1994.

0024-9297/94/2227-5476$04.50/0

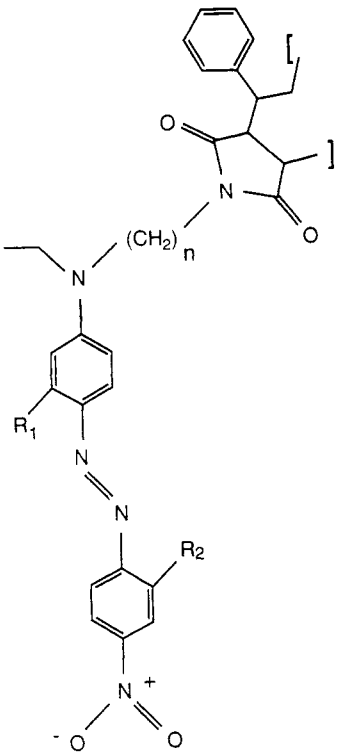

Figure 1. Molecular structure of the modified polyimide NLO polymers.

Table 1. Nomenclature, Azo Dye Substitution Patterns, and Glass Transition Temperatures for the Three Polymers Discussed in This Paper

polymer	n	R_1	R_2	T_g (°C)
A-095.11	3	CH_3	H	137
A-097.07	3	CH_3	Cl	149
A-148.02	2	H	H	172

chromophore loading to the polymer backbone, glass transition temperatures of roughly 140 and 170 °C are achieved with the C_3 and C_2 spacer groups, respectively. The glass transition temperatures of both spacer types extrapolate to ≈218 °C at zero dye content, which is approximately the glass transition temperature of the precursor polymer. As Figures 1 and 2 indicate, the structures of these NLO polymers allow considerable flexibility in the design of materials having both tailored optical and mechanical properties through the use of various chromophores, dye concentrations, and side-chain spacer lengths.

III. Optical Properties

III.a. Absorption. The visible and near IR optical properties of the polymers were measured with a Perkin-Elmer λ9 UV–vis–IR spectrometer. For absorption measurements, we prepared very thin films (90–350 nm) on fused silica substrates in order not to saturate the spectrometer fully in the absorption band of the dyes. The absorption coefficient α cannot be determined from one single measurement since the refractive indices were not determined in this spectral range, and therefore the reflection and transmission coefficients at the different boundaries (see Appendix A) cannot be precisely calculated. We assume that these unknown factors are the same for two films of different thicknesses. The absorption coefficient α can then be calculated by dividing the measured spectra of two films with different thicknesses, as α is then inversely proportional to this difference of thicknesses. Film thicknesses were measured mechanically with an α-stepper profilometer (Tencor 2000) and optically as described in the following section. The values of the film thicknesses obtained from the two measurements were consistent with each other (typically ±10 nm).

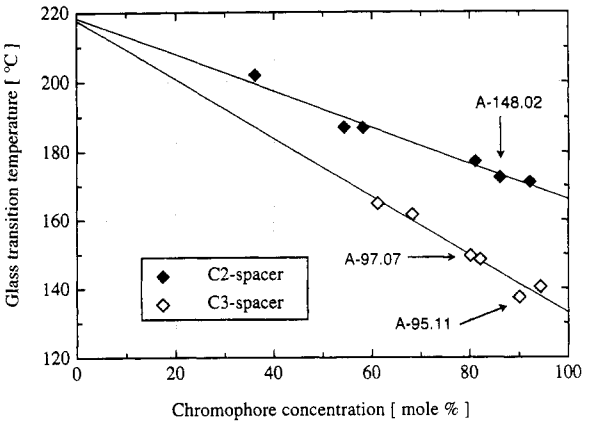

Figure 2. Glass transition temperature as a function of chromophore concentration of the modified polyimide NLO polymers.

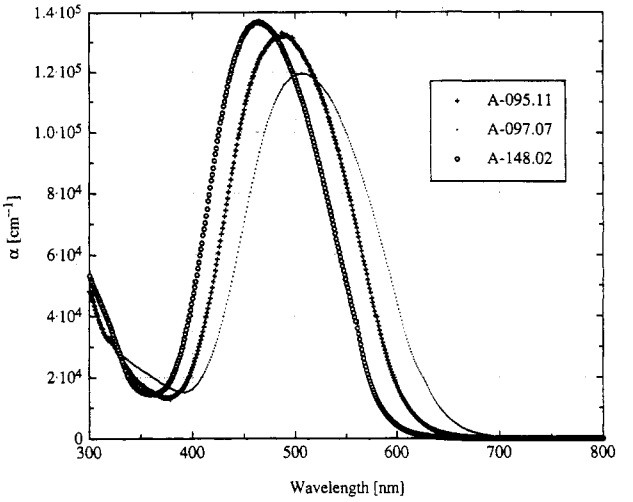

Figure 3. Calculated absorption spectra of A-97.07, A-95.11, and A-148.02 from measurements of two films of different thicknesses.

III.b. Refractive Indices. Several different methods were used to obtain the refractive indices of the different polymers. These include transmission spectroscopy, grating coupling, and attenuated total reflection measurements. Transmission spectroscopy was used for routine characterization as it is fast, simple, and capable of reasonable accuracy. The difference between the refractive indices of the polymer and the substrate (fused silica) produces a modulation of the transmission properties due to optical interference in the thin (≈1 μm) polymeric films. The measured transmissivity is a function of the wavelength, film thickness, and the refractive indices of the substrate, the polymer film, and the covering medium.[17,18] For additional details, see Appendix A. With the known dispersion of the refractive index of the substrate,[19] the complex refractive index of the polymer can be fitted to the measured transmission function. The real part of the polymer refractive index was fitted to a Sellmeier-type dispersion formula,

$$\eta_f^2(\lambda) - 1 = \frac{q}{1/\lambda_o^2 - 1/\lambda^2} + A \qquad (3.1)$$

where λ_o is the absorption wavelength of the dominant

Table 2. Sellmeier Parameters and Refractive Indices at Selected Wavelengths

polymer	A-095.11	A-097.07	A-148.02	method
λ_0 (nm)	491	510	470	
10^6q (nm^{-2})	1.874	1.809	2.074	
A	1.234	1.234	1.234	
n_f (633 nm)[a]	1.84	1.89	1.80	F-P
n_f (1313 nm)[a]	1.65	1.67	1.66	F-P
n_f (1313 nm)[b]		1.663 ± 0.004		grating
n_f (1313 nm)[c]		1.658 ± 0.005		ATR

[a] Uncertainty ±0.01. [b] From grating coupling measurements (TE modes). [c] From attenuated total reflection measurements.

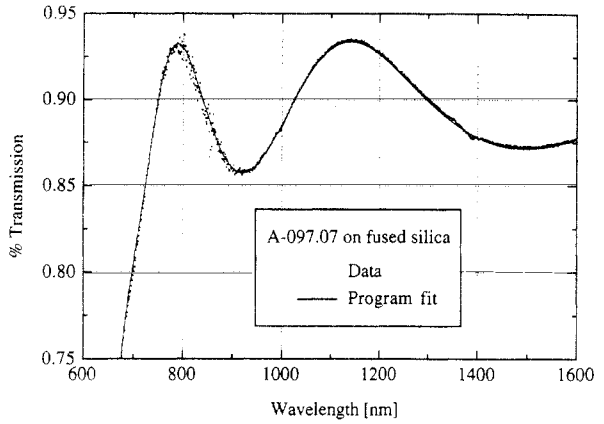

Figure 4. Fabry-Perot interferences of a 678-nm-thick A-097.07 polymer film on a fused silica substrate.

oscillator. The values of λ_0 indicated in Table 2 were obtained directly from the measured absorption curves and kept fixed during fitting the index.

To fit the measured transmission function, an accurate description of the dispersion of the imaginary part of the refractive index, $k_f = \alpha_f\lambda/4\pi$, is also required. Absorption profiles of broadened line shapes can quite often be successfully described by a convolution of the Gaussian and Lorentzian profiles.[20] As these so-called Voigt profiles do not have a simple analytical expression, we used a product of a "stretched" Lorentzian and Gaussian function to describe the imaginary part of the refractive index:

$$k_f(\lambda) = s\frac{\exp(-((1/\lambda_0 - 1/\lambda)/t)^r)}{1 + u(1/\lambda_0 - 1/\lambda)^r} \qquad (3.2)$$

where r, s, t, and u are fitting parameters. We find it to be well suited for the description of the absorption of the film on the long wavelength side of the charge-transfer band. A typical measurement with the fitted transmission function is shown in Figure 4.

Measured refractive indices of the different polymers for films baked at 200 °C for 1 h are summarized in Table 2. This baking procedure was found sufficient to remove any residual solvent in the films. Assuming that the dispersion arising from the chromophores is approximately given by the single oscillator term, the parameter A describes the contribution from the polymer backbone to the refractive index. It was therefore kept constant for all the measurements. This assumption gives a refractive index $n_f = 1.49 \pm 0.02$ for the undoped polymer matrix, which is close to the measured value of 1.52 ± 0.01 (λ = 1313 nm). The difference may arise from the change in the polymer structure once the NLO chromophore is coupled to the polymer backbone. Values obtained from grating coupling measurements or from attenuated total reflection (ATR) measurements are also given, when available.

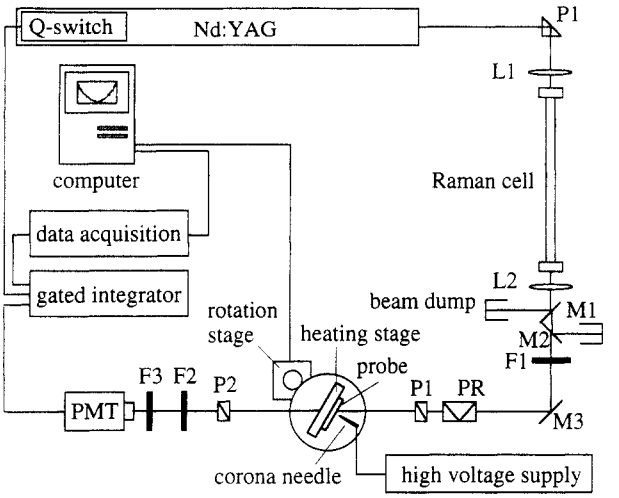

Figure 5. Experimental setup for SHG measurements (Maker fringe technique). The laser beam is focused with lens L1 into a 1-m-long Raman cell (f = 500 mm) and recollimated with lens L2 (f = 500 mm). Dielectric mirrors M1 and M2 reject the fundamental wavelength λ = 1.06 μm. Filter F1 eliminates residual flashlamp light. PR: polarization rotator. Filter F2 blocks the fundamental wave (λ = 1.54 or 1.9 μm), and F3 attenuates the second harmonic signal. Measurements at λ = 1.3 and 1.06 μm are done without a Raman cell.

III.c. Nonlinear Optical Measurements. Nonlinear optical measurements were performed using a standard Maker-fringe technique.[21] Stimulated Raman scattering in compressed H_2 (≈40 bar) and CH_4 (≈20 bar) in approximately 1-m-long gas cells provided the fundamental wavelengths of λ = 1907 nm and λ = 1542 nm, respectively. The experimental setup is shown in Figure 5. The Nd:YAG pump laser (BMI D.N.S 501) at λ = 1064 nm had pulse energies of 200–250 mJ/pulse and pulse durations of about 20 ns. This laser could be operated at λ = 1338 nm by changing the cavity mirrors.

Film Preparation. Films of each polymer with thicknesses ranging from 0.5 to 2.5 μm were spin cast from solutions of cyclopentanone/*N*-methyl-2-pyrrolidone NMP (5:1) of varying polymer concentrations onto ITO-coated glass substrates. Films processed for 1 day at 170 °C or more are called hard baked.

Poling Procedure. Several films of each polymer were poled near the glass transition with a positive or negative corona discharge at voltages between 8 and 15 kV. The distance between the corona needle and the polymer film was approximately 1–2 cm. During the poling process the film was held at a fixed angle of θ = 25° with respect to the laser beam. After a film was poled, the needle was removed and the film was investigated for its second harmonic response by rotating the poling stage perpendicularly to the incoming laser beam. The nonlinear optical coefficients were evaluated using the following formula[21] (see also Appendix B):

$$I_{2\omega}(\theta) = \frac{8}{\epsilon_0 c}d_{31}^2[t_{af}^{\omega}(\theta)]^4 T_{2\omega}(\theta)[t_{sa}^{2\omega}(\theta)]^2 \times p^2(\theta)I_{\omega}^2\left(\frac{1}{n_{2\omega}^2 - n_{\omega}^2}\right)^2 \sin^2\psi \qquad (3.3)$$

where $t_{af}^{\omega}(\theta)$ and $t_{sa}^{2\omega}(\theta)$ are transmission coefficients at the air/film and substrate/air interfaces, $T_{2\omega}(\theta)$ is the second harmonic Fresnel factor, and $p(\theta)$ is a projection factor. The nonlinear optical d coefficients of the polymer films shown in Table 3 were calibrated with respect to the SHG signal of a quartz crystal reference (d_{11} = 0.4 pm/V).[22] Poling with a positive corona gave NLO susceptibilities

Table 3. Nonlinear Optical Susceptibilities d_{31}

	poling condition	λ = 1338 nm	λ = 1542 nm	λ = 1907 nm
	1. A-095.11			
1	hard baked films measured at 80 °C after poling at +8 kV	23 ± 3	15 ± 2	
	2. A-097.07			
1	unbaked films measured at room temperature, 1 day after poling at −15 kV	11 ± 1	6.8 ± 0.7	4.9 ± 0.5
2	hard baked films measured at 80 °C after poling at +8 kV	23 ± 7	14 ± 2	
	3. A-148.02			
1	hard baked films measured at 80 °C after poling at +8 kV	19 ± 5	14 ± 5	

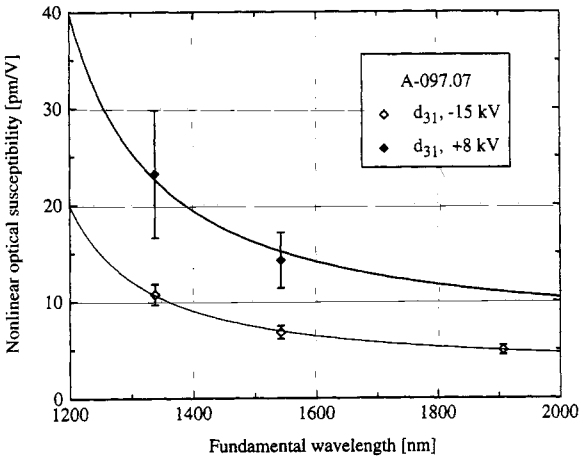

Figure 6. Dispersion of the nonlinear optical susceptibility d_{31} for A-097.07. The solid line is a fit according to the two level model.

approximately twice as high as those obtained from a negative corona, in qualitative agreement with the results of Hampsch et al.[23] At higher than the above mentioned voltages (positive or negative coronas), serious film damage occurred.

Dispersion of the Nonlinear Optical Coefficients. The simple model of noninteracting NLO chromophores leads to the following relation between macroscopic ***d*** values and the microscopic hyperpolarizability, β_{zzz}:[24]

$$d_{ijk} = N f_i^{2\omega} f_j^{\omega} f_k^{\omega} \langle \beta_{zzz} \rangle_{ijk} \tag{3.4}$$

where N is the number density of NLO molecules. The local field factors f express the change in the dielectric environment at the indicated frequency due to the neighboring molecules. The above expression assumes that the dominant term of the hyperpolarizability tensor for molecules with a one-dimensional charge-transfer state along the molecular z-axis is β_{zzz}. Since the orientational averaging of $\langle ... \rangle_{ijk}$ is frequency independent, the dispersion of the nonlinear optical coefficients are primarily given by the dispersion of β_{zzz}.[25] Using the Lorentz approximation for the local field factors, the measured data at different wavelengths can be fitted to the following equation:

$$d_{31}^{-2\omega;\omega;\omega} = \text{const} \frac{n_{2\omega}^2 + 2}{3}\left(\frac{n_\omega^2 + 2}{3}\right)^2 \frac{\omega_0^2}{(\omega_0^2 - 4\omega^2)(\omega_0^2 - 4\omega^2)} \tag{3.5}$$

Since not all the measurements could be finished within 1 day, the results of each measurement were calibrated relative to quartz λ = 1064 nm (d_{11} = 0.4 pm/V)[22] on the same day to prevent errors due to possible orientational relaxations within this period. The results shown in Figure 6 of the dispersion of d_{31} for A-097.07 correspond well to the two level model for the NLO chromophores.

The two level model composed of the highest occupied and lowest unoccupied valence orbitals accurately describes the nonlinear optical response of these azo chromophores. The measured NLO ***d*** coefficients compare well with $LiNbO_3$ but come far short of theoretical optimized values due to inefficient orientation of the chromophores. We estimate that the order induced by the poling field is only about 23% of the optimal orientation possible (see Appendix C). With the use of a corona discharge, it is not clear whether this degree of order can be increased or not, since there is not enough knowledge of the electric fields applied over the polymer films.

Table 4. Electrooptic Coefficients r_{13} at the Wavelength λ = 1313 nm (Modulation Frequency: 1 kHz) and Corresponding Poling Voltages V_p

polymer	r_{13}^e (pm/V)	r_{13}^T (pm/V), V_p (V/μm)
A-095.11[a]	6.0 ± 0.6	6.7 ± 0.4, 150
A-097.07[b]	5.4 ± 1.8	2.3 ± 0.2, 120
A-148.02[a]	5.5 ± 1.3	6.5 ± 0.3, 150

[a] Ellipsometric measurement. [b] Interferometric measurement.

III.d. Electrooptic Measurements. Electrooptic measurements were performed for electric field frequencies much lower than acoustic and vibrational frequencies and evidently than the frequencies of the optical fields. At those low frequencies the free electrooptic coefficient r^T is the sum of the electronic contribution (r^e) and the effects from optic (r^o) and acoustic (r^a) phonons.[26] For polar inorganic materials the last two contributions are very important; however, for organic materials the electrooptic effect is assumed to be mainly of electronic origin.

The electronic contribution to the electrooptic coefficient at low frequencies and the nonlinear optical susceptibilities are directly related by[27]

$$r_{ijk}^e = \frac{-4}{n_i^2 n_j^2} d_{ijk}^{EO} \tag{3.6}$$

The superscript EO denotes the NLO d coefficient extrapolated to zero frequency for the electric modulation field:

$$d_{ijk}^{EO} = d_{ijk}^{-\omega;\omega,0} = \frac{f_i^{\omega} f_j^{\omega} f_k^{0}}{f_k^{2\omega'} f_i^{\omega'} f_j^{\omega'}} \frac{(3\omega_0^2 - \omega^2)(\omega_0^2 - \omega'^2)(\omega_0^2 - 4\omega'^2)}{3(\omega_0^2 - \omega^2)^2 \omega_0^2} d_{kij}^{-2\omega';\omega';\omega'} \tag{3.7}$$

ω' is the optical frequency at which $d_{kij}^{-2\omega';\omega';\omega'}$ is measured and ω is the optical frequency involved in the electrooptic experiment. Therefore, SHG experiments can be used to deduce the electronic part of the EO effect and provide a measure of the expected electrooptic response of a material. Table 4 contains these data for the three polymers investigated in this work.

Measurement of the Electrooptic Coefficient. Either the Michelson interferometric setup depicted in Figure 7a or the ellipsometric technique[28] (Figure 7b) was used to measure the electrooptic coefficient r_{13} of electrode poled films.

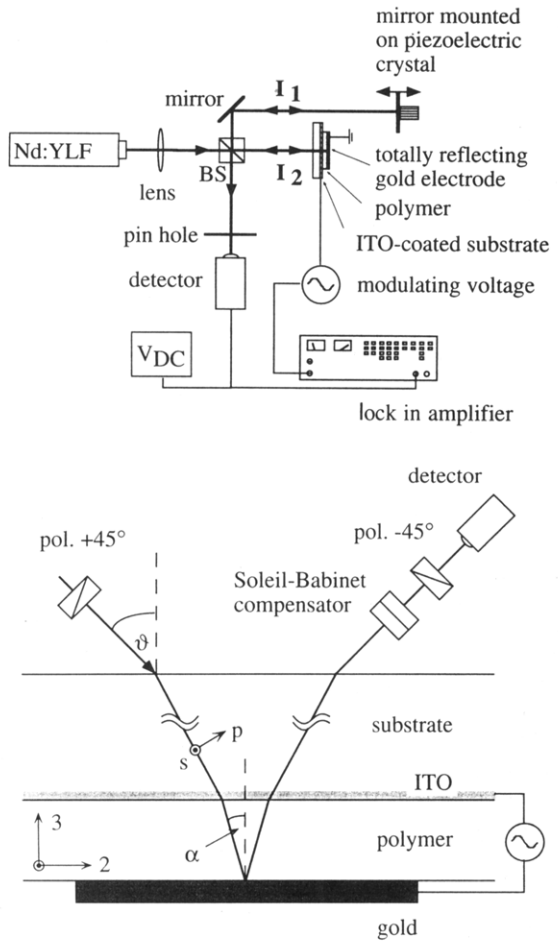

Figure 7. (a, top) Michelson interferometer setup for EO measurements. (b, bottom) Ellipsometric setup for EO measurements.

Films of each NLO polymer ($L \approx 1$ μm) on ITO-coated glass substrates with a 100-nm-thick top gold electrode were poled at T_g for about $^1/_2$ h at poling fields between 120 and 150 V/μm. A diode pumped Nd:YAG laser (λ = 1313 nm) was slightly focused onto the films and the output was detected with an IR sensitive germanium photodiode. A modulation voltage $U_{eff} \leq 10$ V at 1 kHz was applied over the film and used as a reference for a lock-in amplifier. Table 4 gives the results of these measurements together with the expected values from SHG data.

In the *interferometric setup* (Figure 7a) the beam intensity I_1 in the reference arm interferes with the beam of intensity I_2 in the probe arm. The resulting interference pattern at the output is given by

$$I = I_1 + I_2 + 2\sqrt{I_1 I_2}\cos[\Delta\varphi_0 + \delta\varphi(E)] \qquad (3.8)$$

The phase difference $\Delta\varphi_0$ results from different phases acquired by the beams in the two arms and can be adjusted to an odd multiple of $\pi/2$ by moving the piezoelectric mirror. Applying a weak sinusoidal modulating voltage $U = U_0 \sin(2\pi\nu t)$ over the poled polymer film induces an extra phase shift (the beam passes the film twice; therefore an extra factor of 2 in front (see also Appendix D))

$$\delta\varphi(E) = 2\frac{2\pi}{\lambda}\Delta nL = -2\frac{2\pi}{\lambda}\frac{n^3 r}{2}\frac{U_0}{L}L\sin(2\pi\nu t) \qquad (3.9)$$

which modulates the intensity in the following way:

$$I = I_1 + I_2 + 2\sqrt{I_1 I_2}\frac{2\pi}{\lambda}n^3 r U_0 \sin(2\pi\nu t) \qquad (3.10)$$

A lock in amplifier is then used for phase-sensitive detection of the modulation signal, I_{eff},

$$I_{eff} = 2\sqrt{I_1 I_2}\frac{2\pi}{\lambda}n^3 r U_{eff} \quad (U_{eff} = U_0/\sqrt{2}) \qquad (3.11)$$

By introduction of the intensity contrast, $\Delta I = I_{max} - I_{min} = 4\sqrt{I_1 I_2}$, which can be measured with a dc voltmeter at the detector output ($\Delta\varphi_0 = 0$ and π), the electrooptic coefficient is calculated from

$$r_{13} = I_{eff}\frac{\lambda}{\pi n^3 \Delta I U_{eff}} \qquad (3.12)$$

The thickness of the film does not have to be known since the optical path and the electrode spacing are the same.

In the *ellipsometric configuration* (Figure 7b) the input laser beam is polarized at 45° with respect to the plane of incidence and the output intensity is given by

$$I = \Delta I \sin^2[(\Delta\varphi_0 + \delta\varphi_{sp}(E))/2] \qquad (3.13)$$

where $\Delta\varphi_0$ can be set to $\pi/2$ (half intensity output) with a Babinet–Soleil compensator. The intensity contrast is again ΔI. A phase difference $\Delta\varphi_{sp}(E)$ is acquired between the parallel (p) and perpendicular (s) components of the beam as they pass through the polymer film when the modulating field E is on. The phase difference is due to the different effective electrooptic coefficients experienced by the s- and p-polarized waves and the consequent difference in the optical path length l between the two waves in the polymer film:

$$\Delta\varphi_{sp} = \frac{2\pi}{\lambda}(l\delta n_{sp} + n\delta l_{sp}) \qquad (3.14)$$

For small modulation voltages, the modulated signal I_{eff} is then proportional to this phase difference:

$$I_{eff} \approx 1/(2\sqrt{2})\Delta I \delta\varphi_{sp} \qquad (3.15)$$

With the approximation $n_s \approx n_p \approx n$ and the assumption $r_{33} = 3r_{13}$[29] one obtains[28]

$$r_{13} = \frac{\lambda I_{eff}}{2\pi U_{eff}\Delta I n^2}\frac{(n^2 - \sin^2\vartheta)^{3/2}}{(n^2 - 2\sin^2\vartheta)}\frac{1}{\sin^2\vartheta} \qquad (3.16)$$

where ϑ is the external angle of incidence. Again, knowledge of the film thickness is not needed.

Figure 8 shows the representative output characteristics for both kind of experiments: in the interferometric case the function as shown is proportional to $\cos(\Delta\varphi)$ whereas for the ellipsometric experiment it is proportional to $\sin^2(\Delta\varphi/2)$.

For a purely linear electrooptic effect one obtains the same modulated signal at the bias points A and B except for a sign reversal. At point O there should not be any modulation at the same frequency. However, due to multiple reflection and absorption effects in the different layers, the signals in A and B are often not symmetric and one can even measure a modulation at point O. In this case the results have to be interpreted very carefully.[30]

IV. Time–Temperature Relaxation Behavior

As previously mentioned, insufficient temporal stability of poled polymers at elevated temperatures is one factor

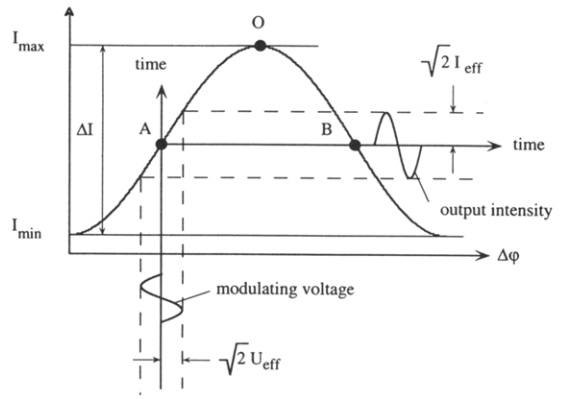

Figure 8. Output characteristic of the Michelson interferometer. A small applied sinusoidal voltage modulates the light intensity around the bias point A.

that precludes the present use of these materials for many potential device applications. Consequently, we have made extensive time–temperature measurements on the relaxational properties of these side-chain NLO polymers in an effort to model and predict their long-term orientational stability. As the stability of the poling induced order within these polymers is to a large extent most strongly coupled with aspects of the glass transition, we first discuss some useful phenomenological relations involving relaxational behavior both above and below T_g in polymeric materials.

IV.a. Phenomenology of the Glass Transition. A variety of theoretical expression exist to describe the temperature dependence of the relaxation time based on free volume, entropy, or other phenomenological expressions.[31] A common feature of these expressions is a partitioning of the relaxation time into an Arrhenius temperature dependent part and a term describing the temperature dependence of the structural relaxation. In the Adam–Gibbs entropic formulation of the glass transition, the structural relaxation time of polymeric liquids involves the cooperative rearrangement of increasingly larger numbers of molecular segments as the temperature decreases.[32,33] Kovacs has shown that these various expressions are equivalent descriptions of the glass transition, within this relaxation region.[31]

As originally proposed by Tool,[34] the structural relaxation of glasses can be described in terms of a fictive temperature, T_f. The value of T_f is typically calculated by the procedure outlined by Narayanaswamy[35] and further developed by Moynihan[36,37] and Hodge.[38] With this description of the glass transition, Hodge has shown that the following expression can be derived for the relaxation time associated with the cooperative chain rearrangements:[39]

$$\tau = A \exp\left(\frac{B}{T(1 - T_2/T_f)}\right) \tag{4.1}$$

where B is an activation energy divided by R, the gas constant, T is the temperature, A is a time parameter discussed below, and T_2 is the temperature at which the configurational entropy of the relaxing molecular segments equals zero; see Figure 9.

Glass transition temperatures and the relaxation behavior of many materials are usually and conveniently measured by DSC techniques. The kinetics of the glass transition, as measured by DSC, has been most successfully modeled in terms of the Adams–Gibbs formulation of the glass transition, as subsequently developed by Scherer[40]

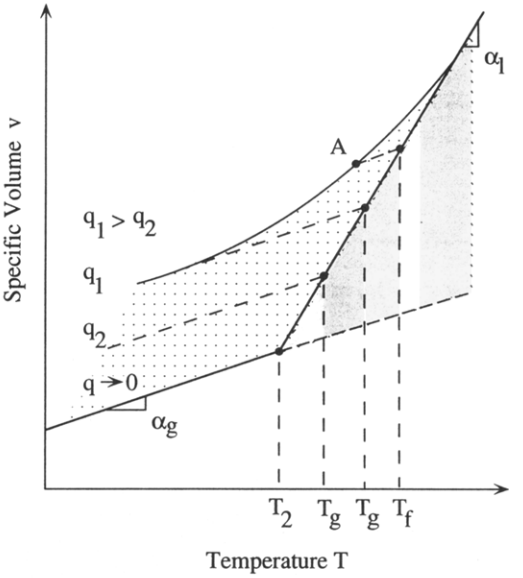

Figure 9. Phenomenology of the glass transition exemplified for the specific volume as a function of temperature. Depending on the rate of cooling q, the system deviates from the liquid equilibrium state to the glassy state at different temperatures due to structural constraints. The glass transition temperature T_g, defined at the intersection point between the glassy and the liquid line, is therefore a kinetic phenomenon. At a given point A, the fictive temperature T_f is constructed as the intersection of the equilibrium line and the line through A with slope α_g, the expansion coefficient for the glass. In simple processes T_f reaches the final value T_g. For infinitely slow cooling the glassy state is a true equilibrium state with transition temperature T_2.

and Hodge.[39,41] Our results on the optimization of the parameters A, B, and T_2, obtained from the DSC data of a number of polymers, indicate that the preexponential time factor A can be replaced by the relation

$$A = \tau_g \exp\left(\frac{-B}{T_g - T_2}\right) \tag{4.2}$$

The relaxation time at any temperature can then be normalized with respect to the relaxation time at the glass transition temperature, $\tau_n = \tau/\tau_g$. Combining this with the above expression for the prefactor A gives the following expression for the normalized relaxation time, τ_n:

$$\ln \tau_n = -\frac{B}{T_g - T_2} + \frac{B}{T(1 - (T_2/T_f))} \tag{4.3}$$

Above the glass transition temperature, $T_f \approx T$ and the preceding expression reduces to the Fulcher–Tammann–Hesse equation,

$$\ln \tau_n = -\frac{B}{T_g - T_2} + \frac{B}{T - T_2} \tag{4.4}$$

in agreement with a large experimental data base of measurements on polymeric materials.[42] Using the Williams–Landel–Ferry (WLF) description of relaxation above the glass transition, the temperature T_2 can be written as $T_2 = T_g - C_2^g$, with $C_2^g \approx 50$ °C if "universal" relaxation behavior is assumed. More realistically, however, universal behavior is not valid and values of C_2^g from mechanical and dielectric measurements of glassy polymers above T_g vary over a considerable range from about 40 to 100 °C.[42]

Below the glass transition, T_f reaches a final limiting value approximately equal to T_g in simple cooling processes, i.e. without sub-T_g annealing. We approximate

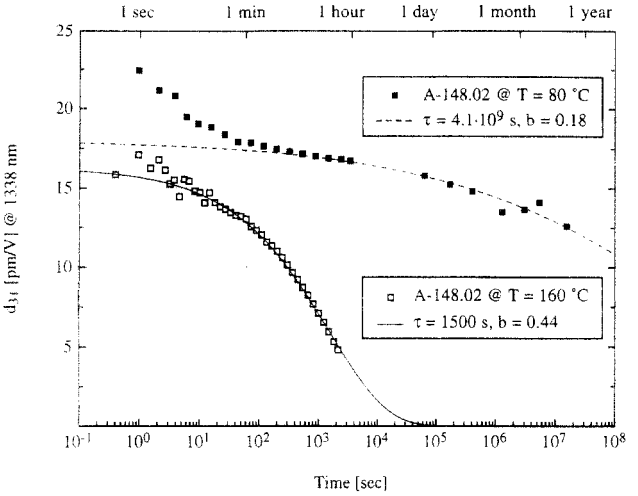

Figure 10. Orientational relaxation of the nonlinear optical susceptibility of A-148.02 as measured by SHG at two different temperatures.

this final T_f by T_g, giving the following temperature dependence of the normalized relaxation time:

$$\ln \tau_n \approx \frac{B}{T_g - T_2}\frac{T_g - T}{T} = 2.303C_1^g\frac{T_g - T}{T} \qquad (4.5)$$

where $2.303C_1^g = B/(T_g - T_2)$ is the other WLF parameter. Equation 4.5 is equivalent to an Arrhenius temperature dependence of the α relaxation processes associated with the large-scale polymer chain motion at temperatures below the glass transition.

IV.b. Long-Term Stability of Poled Polymers. Relaxation of the side-chain chromophores below the glass transition was investigated by the decay of the SHG signal from corona poled films. After poling near the glass transition temperature, the polymer films were cooled at a rate of ≈2–5 °C/min to the decay temperature which was chosen to be in the range from 70 to 145 °C. At this temperature the corona field was turned off and the SHG signal was continuously monitored for a time period of 14–100 h depending on the decay temperature. An 800-Hz Q-switched Nd:YAG laser operating at 1313 nm was used for the SHG decay experiments. The SHG signal was detected with a PMT and a boxcar averager with a 1-s integration time and active baseline subtraction. A quartz reference signal was monitored concurrently to reduce laser fluctuations and correct for possible drifts in the laser intensity level over the long acquisition times involved in the decay measurements.

The time dependence of the SHG decay due to orientational relaxation of the NLO chromophores was usually found to be well represented by a Kohlrausch–Williams–Watts (KWW) stretched exponential function,

$$\boldsymbol{d}(t) = \boldsymbol{d}_0 \exp\left[-(t/\tau)^b\right] \qquad (4.6)$$

where $0 < b \leq 1$ is a measure of the breadth of the distribution function and the extent of deviation from single exponential behavior. The characteristic relaxation time τ is the time that is required for the NLO $\boldsymbol{d}$ coefficient to decay to $1/e$ of its initial value.

Figure 10 shows examples of the decay curves for polymer A-148.02 at two different decay temperatures in a semilogarithmic plot, which is the most appropriate representation for this kind of relaxation. All of the decay experiments exhibit a fast initial decay amounting to about 20–30% of the total initial SHG signal during the first 1–10 min. We attribute this decay to the release of charge carriers trapped in the film after the corona voltage has been turned off. In most cases the contribution from this fast decay has been isolated by introducing in eq 4.6 an extra fit parameter t_0 which provides a time offset. The result of this procedure is demonstrated in Figure 10 for the case of SHG decay of A-148.02 at 80 °C; it is evident from the fit which points at the beginning of the decay should be eliminated from subsequent data analysis.

Table 5. SHG Relaxation Times τ at 80 °C

polymer	log τ (s)	$10^{-7}\tau$ (s)
A-095.11	7.7 ± 0.3	4.6
A-097.07	7.9 ± 0.3	7.8
A-148.02	9.5 ± 0.5	350

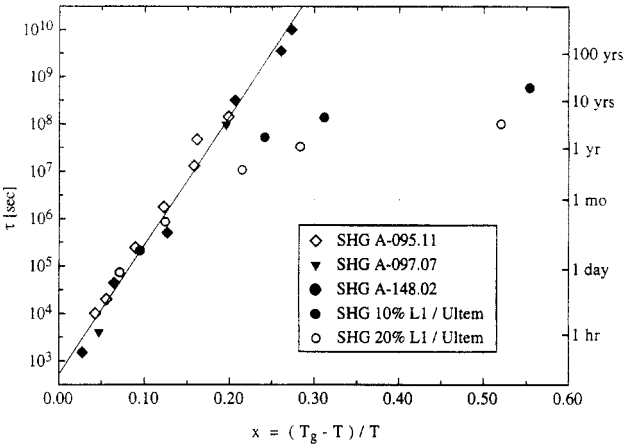

Figure 11. Scaling of relaxation times with $(T_g - T)/T$. The solid line is fitted to the SHG decay data of the polyimide side-chain polymers by assuming an Arrhenius type decay law: log $\tau = 2.7 + 27x$.

The nonlinear optical susceptibilities $\boldsymbol{d}_0$ at 80 °C given in Table 3 were obtained with this fitting procedure. The relaxation times obtained for τ range from a few minutes at temperatures near T_g to several years at the lowest temperatures measured ($\approx T_g - 70$ °C). For temperatures lower than 20 deg below T_g, the SHG decay exhibits Arrhenius behavior with activation energies of about 220–250 kJ/mol. Best fit values for b range from 0.15 to 0.50, with lower values (broader distributions) at lower temperatures.

Reliable prediction of the KWW functional exponent b of the NLO or EO effect is hampered by the difficulty of determining the initial NLO coefficient $\boldsymbol{d}_0$. At high electric field strengths and particularly with the corona fields used in this work, the intense electric field produces frequency doubling via a third-order nonlinear optical effect described by $\chi^{(3)}(-2\omega;\omega,\omega,0)$. With corona fields, charges are also deposited on the polymer surface and injected into the polymer film. Both of these effects decay fairly rapidly compared to the decay of the induced orientational order of the chromophores. However, their presence obscures an assignment of the initial value of the NLO coefficients given by $\chi^{(2)}(-2\omega;\omega,\omega)$. For practical purposes, the subsequent relaxation from perhaps 1 day after poling would be of more value, although, for theoretical modeling, the best estimate for the true initial NLO coefficient is needed. The procedure described above allows us to obtain a reasonably good estimate of these values from corona poled films.

The results of SHG measurements of A-095.11 and A-148.02 below T_g are plotted in Figure 11 using the scaling relation derived in eq 4.5. For purposes of comparison, the results of Stähelin et al.[13] of SHG relaxation measure-

ments of guest–host NLO polymer matrices (Lophine dyes doped in the polyimide Ultem) are also included. The scaling result indicates that the relaxation time below the glass transition associated with the α processes or main-chain segmental motion should be linear with $(T_g - T)/T$ with a slope given by $B/(T_g - T_2) = 2.303C_1^g$. For the side-chain polyimide polymers investigated here, the SHG measurements give a value of $C_1^g \approx 27$, while the "universal" value is ≈ 18. The SHG relaxation data also indicate that the relaxation times of the NLO chromophore of side-chain polymers such as A-095.11 and A-148.02 correlate better with this main-chain segmental motion than do guest–host NLO polymer matrices (similar results for acrylic side-chain NLO polymers have been obtained by Walsh et al.[43]). All of the SHG data, however, appear to be approximately linear within the temperature range from T_g to $T_g - 50$ °C. At lower temperatures, the guest–host polymer systems show strong deviations from linear behavior (see also Stähelin et al.[44]). Furthermore, high dye loading of guest–host systems would appear to introduce additional relaxation mechanisms that destabilize the induced poling order. Errors in the extrapolation of the measured SHG relaxation times may prevent a conclusive interpretation of this kind, however.

Further work is in progress to assess the influence of physical aging on the relaxational properties of NLO chromophores in these polymers.

V. Conclusions

Optical and nonlinear optical measurements on novel modified polyimide side-chain polymers with high glass transition temperatures up to 172 °C have been presented. Using azo chromophores as the NLO side-chain element, high NLO susceptibilities d_{31} = 23 pm/V and EO coefficients r_{13} = 6.5 pm/V at λ = 1.3 μm with electric poling fields up to 150 V/μm could be achieved. These values compare very favorably with other guest–host and functionalized NLO polymers.[45] The increased glass transition temperatures of these novel polyimide polymers represents a significant improvement over more traditional methacrylic NLO systems as a considerable increase in the long-term nonlinear orientational stability is observed.

Phenomenological theories of the glass transition allow us to model some aspects of the chromophore relaxation in these NLO polymers. These theories predict an Arrhenius type temperature dependence below the glass transition for the α processes which can be assumed to be associated with the large-scale molecular motions of the polymeric chains. For temperatures in the range of about $T_g \pm 50$ °C, relaxation of NLO chromophores appears to be primarily influenced by these α type relaxation processes.

We propose a normalized relaxation law with $(T_g - T)/T$ as the relevant scaling parameter. This may be considered "universal" in the sense that the relaxation in several types of polymer systems, side-chain polyimides as well as guest–host systems with greatly differing glass transition temperatures were found to scale well with regard to this parameter in the temperature range of T_g to about T_g – 50 °C. Far below T_g other relaxation mechanisms become increasingly important with decreasing temperatures. Relaxation processes emerge that are dependent on local interactions such as the nature of the dye—polymer molecular bonding, dye concentration, dye size and structure, etc. that are not described by the present model.

Burland et al.[46] found from their experiments on guest–host systems that the temperature dependence of the relaxation time *below* T_g for a variety of polymer hosts is well described by

$$\tau(T) = A' \exp\left(\frac{B'}{T_0' - T}\right) \tag{5.1}$$

with $T_0' = T_g + (50 \pm 10)$ °C. Data points from all guest–host systems lie more or less on the same straight line in the corresponding "scaling plot". However, for PMMA-based side-chain polymers strong deviation was found for temperatures below T_g – 50 °C.[46] We would observe the same phenomenon in such a plot with the polymers described in this paper. Equation 5.1 is an empirical expression: it appears that the value T_g + const was chosen in analogy to the WLF equation. However, this value is arbitrary, since choosing T_g + 100 °C for T_0' would give a "scaling plot" where points from both guest–host and side-chain polymers would lie on a straight line. In contrast to this work, we believe that the constant A in eq 4.2 can be expressed in terms which are physically meaningful, leading to our prediction for the temperature dependence of relaxation times given by eq 4.5.

The polyimide side-chain polymers investigated in this work are found to have significantly improved orientational stability compared to guest–host type polymer systems with the same glass transition temperature. A side-chain polymer with T_g = 170 °C is predicted to have a relaxation time of about 3 years at an operating temperature of 100 °C.

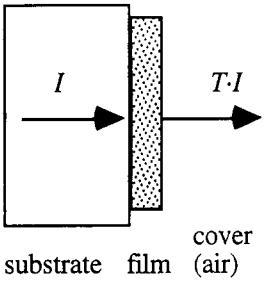

Figure 12. Measurement geometry as used for the determination of refractive indices.

VI. Acknowledgments

We thank U. Stalder, R. Iseli, and G. Recoque for their help with the experiments. J. Söchtig of the Paul Scherrer Institute—Zürich provided helpful assistance with the electrode poling of the polymer films.

Appendix A

Including multiple internal reflections in the film, the transmissivity for an absorbing film with a complex refractive index $(n_f + ik_f)$ on a transparent substrate (index n_s) at normal incidence for the configuration in Figure 12 is given by[47]

$$T = \frac{n_c}{n_s}|t|^2 \tag{A1}$$

where t is the transmission coefficient for the transmitted electric field:

$$|t|^2 = [\tau_{sf}^2\tau_{fc}^2 \exp(-(4\pi/\lambda)k_f h)]/[1 + \rho_{sf}^2\rho_{fc}^2 \exp(-(8\pi/\lambda)k_f h) + 2\rho_{sf}\rho_{fc} \exp(-(4\pi/\lambda)k_f h) \cos(\varphi_{sf} + \varphi_{fc} + (4\pi/\lambda)n_f h)] \tag{A2}$$

The absolute value and the phase of the reflection coefficient at corresponding interfaces is given by ρ and ϕ, and τ is the absolute value of the transmission coefficient.

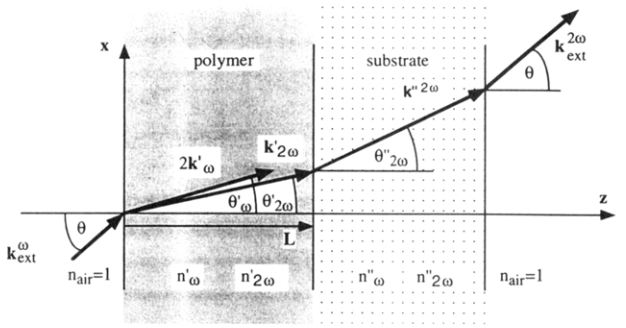

Figure 13. Nomenclature of angles and refractive indices for a sample configuration with air/nonlinear optical polymer/substrate/air interfaces.

The wavelength is denoted by λ and the thickness of the polymer film, by h. At normal incidence the phase, reflection, and transmission coefficients are given by ($n_c = 1$ for air)

$$\rho_{sf}^2 = \frac{(n_s - n_f)^2 + k^2}{(n_s + n_f)^2 + k_f^2} \qquad \tan\varphi_{sf} = \frac{2k_f n_s}{n_f^2 + k_f^2 - n_s^2}$$

$$\rho_{fc}^2 = \frac{(1 - n_f)^2 + k_f^2}{(1 + n_f)^2 + k_f^2} \qquad \tan\varphi_{fc} = \frac{2k_f}{n_f^2 + k_f^2 - 1} \quad \text{(A3)}$$

$$\tau_{sf}^2 = \frac{(2n_s)^2}{(n_s + n_f)^2 + k_f^2} \qquad \tau_{fc}^2 = \frac{4(n_f^2 + k_f^2)}{(1 + n_f)^2 + k_f^2}$$

For the overall transmissitivity there has to be taken into account an additional transmission factor for the first air–substrate interface.

Appendix B

The following remarks about the theory of the Maker fringe technique all refer to Figure 13. The electric field E_ω of the incoming laser beam induces a nonlinear polarization in the poled polymer film

$$P_i'^{2\omega} = \epsilon_0 d_{ijk} E_j'^{\omega} E_k'^{\omega} \quad \text{(B1)}$$

This nonlinear polarization acts as a source term in the wave equation for the field $E^{2\omega}$ at the frequency 2ω. The solution of this wave equation consists of a freely propagating and a bound wave within the active layer:

$$\boldsymbol{E}'_{2\omega} = \boldsymbol{e}_f E'_f \exp(i\boldsymbol{k}'_{2\omega}\boldsymbol{r}) + \boldsymbol{e}_b \frac{P'_{2\omega}/\epsilon_0}{n_\omega^2 - n_{2\omega}^2} \exp(2i\boldsymbol{k}'_{\omega}\boldsymbol{r}) \quad \text{(B2)}$$

where $\boldsymbol{e}_f$ and $\boldsymbol{e}_b$ stand for unit vectors of the free and bound wave. Taking into account the continuity conditions at the first air/film boundary, one finds that

$$E'_f = -\frac{b_x + n'_\omega \cos\theta(p_x \cos\theta'_\omega - p_z \sin\theta'_\omega)}{\cos\theta'_{2\omega} + n'_{2\omega}\cos\theta} \frac{P'_{2\omega}/\epsilon_0}{n_\omega^2 - n_{2\omega}^2} \quad \text{(B3)}$$

Here, b_x is the projection of $\boldsymbol{e}_b$ onto the x-axis and it is given by

$$b_x = p_x - \frac{n_\omega^2}{n_{2\omega}^2} \sin\theta'_\omega (p_x \sin\theta'_\omega + p_z \cos\theta'_\omega) \quad \text{(B4)}$$

In order to calculate the field $E''_{2\omega}$ in the substrate, the continuity relations at the boundary film/substrate must be evaluated:

$$E''_{2\omega} \exp(i2\boldsymbol{k}'_\omega \boldsymbol{L}) = \frac{2n'_{2\omega}\cos\theta'_{2\omega}}{n'_{2\omega}\cos\theta''_{2\omega} + n''_{2\omega}\cos\theta'_{2\omega}} E'_f \exp(i\boldsymbol{k}'_{2\omega}\boldsymbol{L}) + \frac{n'_{2\omega} b_x + n'_\omega \cos\theta'_{2\omega}(p_x \cos\theta'_\omega - p_z \sin\theta'_\omega)}{n'_{2\omega}\cos\theta''_{2\omega} + n''_{2\omega}\cos\theta'_{2\omega}} \times \frac{P'_{2\omega}/\epsilon_0}{n_\omega^2 - n_{2\omega}^2} \exp(i2\boldsymbol{k}'_\omega \boldsymbol{L}) \quad \text{(B5)}$$

When it is assumed that there are no further contributions to the second harmonic signal from the substrate, the resulting intensity in air follows from

$$I_{2\omega}^{air} = \frac{\epsilon_0 c}{2} (t_{sa}^{2\omega} |\boldsymbol{E}''_{2\omega}|)^2 \quad \text{(B6)}$$

For light polarized in the plane of incidence (xz-plane), the transmission coefficient from the substrate to air is given by

$$t_{sa}^{2\omega}(\theta) = \frac{2n''_{2\omega}\cos\theta''_{2\omega}}{\cos\theta''_{2\omega} + n''_{2\omega}\cos\theta} \quad \text{(B7)}$$

Substituting eq B3 for E'_f in eq B5 and calculating the intensity according to eq B6 leads to

$$I_{2\omega}^{air}(\theta) = \frac{\epsilon_0 c}{2} T_{2\omega}(\theta) [t_{sa}^{2\omega}(\theta)]^2 \left(\frac{P'_{2\omega}/\epsilon_0}{n_\omega^2 - n_{2\omega}^2}\right)^2 4\sin^2\psi \quad \text{(B8)}$$

The second harmonic Fresnel factor is abbreviated as

$$T_{2\omega}(\theta) = 2n'_{2\omega}\cos\theta'_{2\omega} \frac{b_x + n'_\omega \cos\theta(p_x \cos\theta'_\omega - p_z \sin\theta'_\omega)}{\cos\theta'_{2\omega} + n'_{2\omega}\cos\theta} \times \frac{n'_{2\omega} b_x + n'_\omega \cos\theta'_{2\omega}(p_x \cos\theta'_\omega - p_z \sin\theta'_\omega)}{(n'_{2\omega}\cos\theta''_{2\omega} + n''_{2\omega}\cos\theta'_{2\omega})^2} \quad \text{(B9)}$$

To get the final result of eq 3.3 the nonlinear polarization $P_i'^{2\omega}$ has to be specified for a uniaxially poled polymer. The poling field in the z-direction imposes an ∞mm point group symmetry on the system and therefore $P_i'^{2\omega}$ is of the form

$$\boldsymbol{P}'_{2\omega} = \epsilon_0 E'^2_\omega \begin{pmatrix} 0 \\ 0 \\ d_{31} \end{pmatrix} \text{ for s-polarized and}$$

$$\boldsymbol{P}'_{2\omega} = \epsilon_0 E'^2_\omega \begin{pmatrix} -2d_{31}\sin\theta'_\omega\cos\theta'_\omega \\ 0 \\ d_{31}\cos^2\theta'_\omega + d_{33}\sin^2\theta'_\omega \end{pmatrix} \quad \text{(B10)}$$

for p-polarized fundamental waves (waves perpendicular to (s) and in the plane (p) of incidence). Assuming nonabsorbing materials at both wavelengths one can set d_{15} equal to d_{31} (Kleinman symmetry). As can be seen from eq B10, only d_{31} can be measured directly (in the s-polarization configuration). Since all quantities in eq B10 refer to the polymer film, they have to be calculated from the fields outside of it:

$$E'^2_\omega = t_{af}^2 E_\omega^2$$

In the case of p-polarized light one has

$$t_{af}^{\omega}(\theta) = \frac{2\cos\theta}{n_{\omega}'\cos\theta + \cos\theta_{\omega}'} \quad \text{(B11)}$$

whereas for an s-polarized incident wave (perpendicular to the plane of incidence)

$$t_{af}^{\omega}(\theta) = \frac{2\cos\theta}{n_{\omega}'\cos\theta_{\omega}' + \cos\theta} \quad \text{(B12)}$$

The oscillating term in eq B8 is due to the interference of the free and bound wave in the polymer:

$$\sin^2\psi = \sin^2\left[\frac{(\boldsymbol{k}_{2\omega}' - 2\boldsymbol{k}_{\omega}')\boldsymbol{L}}{2}\right] = \sin^2\left[\frac{2\pi L}{\lambda}(n_{\omega}'\cos\theta_{\omega}' - n_{2\omega}'\cos\theta_{2\omega}')\right] = \sin^2\left[\frac{\pi L}{2l_c(\theta)}\right] \quad \text{(B13)}$$

For coherence lengths $l_c(0) \equiv l_c \ll L$, $\sin^2\psi$ can be expanded in a power series:[48]

$$\sin^2\psi \approx \left(\frac{\pi}{2}\frac{L}{l_c}\frac{(n_{\omega} + n_{2\omega})/2}{[(n_{\omega}^2 + n_{2\omega}^2)/2 - \sin^2\theta]^{1/2}}\right)^2 \quad \text{(B14)}$$

with the advantage that no difference of refractive indices have to be known.

Appendix C

According to eq 3.4 the maximal $\boldsymbol{d}$ value for optimal orientation is just

$$d_{33}^{\max} = N f_3^{2\omega} f_3^{\omega} f_3^{\omega} \beta_{zzz} \quad \text{(C1)}$$

since the orientational averaging for the microscopic hyperpolarizability equals 1.

Taking for β_{zzz} of A-148.02 the value for Disperse Red 1 (DR1) from Cheng et al.[49] and correcting for dispersion leads to $\beta_{zzz} = 315 \times 10^{-40}$ m^4/V at $\lambda = 1338$ nm. The number density of NLO molecules

$$N = \frac{\rho}{M} N_A \quad \text{(C2)}$$

where N_A is Avogadro's number, is calculated by assuming a density $\rho = 1.4$ g/cm^3 and a molecular weight $M = 456$. Together with the local field factors, this gives an optimal nonlinear optical susceptibility $d_{33}^{\max} = 249$ pm/V for A-148.02 at $\lambda = 1338$ nm. This value has to be compared to $d_{33} = 57$ pm/V as measured for A-148.02 by assuming that $d_{33} = 3d_{31}$.[29]

Appendix D

Since poled films are uniaxial with the optic axis perpendicular to the film plane, the index ellipsoid is of the form

$$\left(\frac{1}{n^2}\right)_{ij} x_i x_j = \frac{x_1^2}{n_0^2} + \frac{x_2^2}{n_0^2} + \frac{x_3^2}{n_e^2} = 1 \quad \text{(D1)}$$

The highest symmetry axis x_3 points into the poling direction. An applied dc field E distorts the index ellipsoid in the following way:

$$\left[\left(\frac{1}{n^2}\right)_{ij} + \Delta\left(\frac{1}{n^2}\right)_{ij}\right] x_i x_j = 1 \quad \text{with} \quad \Delta\left(\frac{1}{n^2}\right)_{ij} = r_{ijk}E_k \quad \text{(D2)}$$

The linear electrooptic or Pockels tensor elements, r_{ijk}, describe the field induced refractive index change. In the case of a poled polymer film (∞mm symmetry) this leads to (again in the contracted tensor notation r_{uk}, since r_{ijk} is symmetric in its first two indices)

$$\frac{x_1^2 + x_2^2}{n_0^2} + \frac{x_3^2}{n_e^2} + r_{13}E_3(x_1^2 + x_2^2) + r_{33}E_3x_3^2 = 1 \quad \text{(D3)}$$

for a dc field E_3 in the poling direction. The field induced change in the ordinary refractive index to first order is given by

$$\left.\begin{aligned} \frac{1}{n_o^2(E_3)} &= \frac{1}{(n_o + \Delta n_o)^2} \cong \frac{1}{n_o^2}\left(1 - 2\frac{\Delta n_o}{n_o}\right) \\ \frac{1}{n_o^2(E_3)} &= \frac{1}{n_o^2} + r_{13}E_3 \end{aligned}\right\} \Delta n_o \cong -\frac{n_o^3}{2} r_{13}E_3 \quad \text{(D4)}$$

This calculation is also valid for the field induced change in the extraordinary refractive index.

VII. References

(1) Lytel, R.; Lipscomb, G. F.; Kenney, J. T.; Binkley, E. S. In *Polymers for Lightwave and Integrated Optics*; Hornack, L. A., Ed.; Marcel Dekker: New York, 1992.
(2) See for example: *Organic Thin Films for Photonic Applications*; Technical Digest Series Vol. 17; Optical Society of America: Washington, DC, 1993.
(3) Man, H.-T.; Yoon, H. N. *Adv. Mater.* **1992**, *4*, 159.
(4) Eich, M.; Reck, B.; Yoon, D. Y.; Willson, C. G.; Bjorklund, C. G. *J. Appl. Phys.* **1989**, *66*, 3241–3247.
(5) Mandal, B. K.; Chen, Y. M.; Lee, J. Y.; Tripathy, J. K. *Appl. Phys. Lett.* **1991**, *58*, 2459.
(6) Müller, H.; Müller, I.; Nuyken, O.; Strohriegl, P. *Makromol. Chem. Rapid Commun.* **1992**, *13*, 289.
(7) Zhu, X.; Chen, Y. M.; Li, L.; Jeng, R. J.; Mandal, B. K.; Kumar, J.; Tripathy, S. K. *Opt. Commun.* **1992**, *88*, 77–80.
(8) Chen, M.; Yu, L.; Dalton, L. R.; Shi, Y.; Steier, W. H. *Macromolecules* **1991**, *24*, 5421–5428.
(9) Lin, J. T.; Hubbard, M. A.; Marks, T. J.; Lin, W.; Wong, G. K. *Chem. Mater.* **1992**, *4*, 1148.
(10) Köhler, W.; Robello, D. R.; Dao, P. T.; Willand, C. S.; Williams, D. J. *J. Chem. Phys.* **1990**, *93*, 9157.
(11) Wu, J.; Valley, J. F.; Ermer, S.; Binkley, E. S.; Kenney, J. T.; Lipscomb, G. F.; Lytel, R. *Appl. Phys. Lett.* **1991**, *58*, 225–227.
(12) Wu, J. W.; Binkley, E. S.; Kenney, J. T.; Lytel, R.; Garito, A. F. *J. Appl. Phys.* **1991**, *69*, 7366–7368.
(13) Stähelin, M.; Burland, D. M.; Ebert, M.; Miller, R. D.; Smith, B. A.; Twieg, R. J.; Volksen, W.; Walsh, C. A. *Appl. Phys. Lett.* **1992**, *61*, 1626.
(14) Rao, V. P.; Jen, A. K. Y.; Wong, K. Y.; Drost, K.; Mininni, R. M. *Nonlinear optical properties of organic materials V*; SPIE: Bellingham, WA, 1992; Vol. 1775, pp 32–42.
(15) Jen, A. K. Y.; Wong, K. Y.; Drost, K.; Rao, V. P.; Caldwell, B.; Mininni, R. M. *Organic Thin Films for Photonic Applications*; Technical Digest Series Vol. 17; Optical Society of America: Washington, DC, 1993; 286 paper FB3-1.
(16) Ahlheim, M.; Lehr, F. *Makromol. Chem.* **1994**, *195*, 361.
(17) Manificier, J. C.; Gasiot, J.; Fillard, J. P. *J. Phys. E: Sci. Instrum.* **1976**, *9*, 1002–1004.
(18) Swanepoel, R. *J. Phys. E: Sci. Instrum.* **1983**, *16*, 1214–1222.
(19) Gray, D. E. *American Institute of Physics Handbook*; AIP: New York, Oxford, U.K., 1972.
(20) Loudon, R. *The quantum theory of light*, 2nd ed.; Oxford University Press: Oxford, U.K., 1983.
(21) Jerphagnon, J.; Kurtz, S. K. *J. Appl. Phys.* **1970**, *41*, 1667.
(22) Landolt-Börnstein. *Elastische, piezoelektrische, pyroelektrische, piezooptische Konstanten und nichtlineare dielektrische Suszeptibilitäten von Kristallen*; Springer: Berlin, 1979.
(23) Hampsch, H. L.; Torkelson, J. M.; Bethke, S. J.; Grubb, S. G. *J. Appl. Phys.* **1990**, *67*, 1037–1041.
(24) Zyss, J.; Oudar, J. L. *Phys. Rev.* **1982**, *A26*, 2028–2048.

(25) Oudar, J. L. *J. Chem. Phys.* **1977**, *67*, 446.
(26) Bosshard, C.; Sutter, K.; Schlesser, R.; Günter, P. *J. Opt. Soc. Am.* **1993**, *B10*, 867.
(27) Boyd, G. D.; Kleinman, D. A. *J. Appl. Phys.* **1968**, *39*, 3597–3639.
(28) Teng, C. C.; Man, T. H. *Appl. Phys. Lett.* **1990**, *56*, 1734–1736.
(29) Singer, K. D.; Kuzyk, M. G.; Sohn, J. E. *J. Opt. Soc. Am. B* **1987**, *4*, 968–976.
(30) Levy, Y.; Dumont, M.; Chastaing, E.; Robin, P.; Chollet, P. A.; Gadret, G.; Kajzar, F. *Mol. Cryst. Liq. Cryst. Sci. Technol., Sect. B* **1993**, *4*, 1–19.
(31) Kovacs, A. J.; Hutchinson, J. M.; Aklonis, J. J. In *The Structure of Non-Cristalline Materials*; Gaskell, P. H., Ed.; Taylor and Francis: London, 1977.
(32) Gibbs, J. H.; DiMarzio, E. A. *J. Chem. Phys.* **1958**, *28*, 373.
(33) Adam, G.; Gibbs, J. H. *J. Chem. Phys.* **1965**, *43*, 139–145.
(34) Tool, A. Q. *J. Am. Ceram. Soc.* **1946**, *29*, 240.
(35) Narayanaswamy, O. S. *J. Am. Ceram. Soc.* **1971**, *54*, 471.
(36) Moynihan, C. T.; Macedo, P. B.; Montrose, C. J.; Gupta, P. K.; DeBolt, M. A.; Dill, J. F.; Drake, P. W.; Easteal, A. J.; Wlterman, P. B.; Moeller, R. P.; Sasabe, H.; Wilder, J. A. *Ann. N.Y. Acad. Sci.* **1976**, *279*, 15.
(37) DeBolt, M. A.; Easteal, A. J.; Macedo, P. B.; Moynihan, C. T. *J. Am. Ceram. Soc.* **1976**, *59*, 16.
(38) Hodge, I. M.; Berens, A. R. *Macromolecules* **1982**, *15*, 762.
(39) Hodge, I. M. *Macromolecules* **1986**, *19*, 936.
(40) Scherer, G. W. *J. Am. Ceram. Soc.* **1984**, *67*, 504.
(41) Hodge, I. M. *J. Non-Cryst. Solids* **1991**, *131–133*, 435.
(42) Ferry, J. D. *Viscoelastic Properties of Polymers*, 3rd ed.; J. Wiley & Sons: New York, 1980.
(43) Walsh, C. A.; Burland, D. M.; Lee, V. Y.; Miller, R. D.; Smith, B. A.; Twieg, R. J.; Volksen, W. *Macromolecules* **1993**, *26*, 3720–3722.
(44) Stähelin, M.; Walsh, C. A.; Burland, D. M.; Miller, R. D.; Twieg, R. J.; Volksen, W. *J. Appl. Phys.* **1993**, *73*, 8471–8479.
(45) Nahata, A.; Shan, J.; Yardley, J. T.; Wu, C. *J. Opt. Soc. Am.* **1993**, *B10*, 1553–1564.
(46) Burland, D. M.; Miller, R. D.; Walsh, C. A. *Chem. Rev.* **1994**, *94*, 31–75.
(47) Born, M.; Wolf, E. *Principles of Optics*, 6th ed.; Pergamon Press: Oxford, U.K., 1980.
(48) Kuzyk, M. G.; Singer, K. D.; Zahn, H. E.; King, L. A. *J. Opt. Soc. Am.* **1989**, *B6*, 742.
(49) Cheng, L. T.; Tam, W.; Stevenson, S. H.; Meredith, G. R.; Rikken, G.; Marder, S. *J. Phys. Chem.* **1991**, *95*, 10631–10643.